Macromolecules
ARTICLE

Macromolecules **2009**, *42*, 8187–8197 **8187**
DOI: 10.1021/ma901359x

Ring-Opening Polymerization of L,L-Lactide: Kinetic and Modeling Study

Yingchuan Yu,[†] Giuseppe Storti,[‡] and Massimo Morbidelli*,[†]

[†]*Institute for Chemical and Bioengineering, Department of Chemistry and Applied Biosciences, Swiss Federal Institute of Technology (ETH), 8093 Zurich, Switzerland, and* [‡]*Dipartimento di Chimica, Materiali e Ingegneria Chimica "Giulio Natta", Politecnico di Milano, 20131 Milan, Italy*

Received June 25, 2009; Revised Manuscript Received September 22, 2009

ABSTRACT: Ring-opening polymerization of L,L-lactide with various amounts of catalyst, 2-ethylhexanoic acid tin(II) salt, and cocatalyst, 1-dodecanol, at 130 °C in bulk is examined. Monomer-to-catalyst and cocatalyst-to-catalyst molar ratios were changed from 500 to 4000 and from 1 to 600, respectively. In agreement with previous literature, the catalyst concentration is affecting the reaction rate, whereas OH-bearing species (such as cocatalyst and impurities) are controlling both reaction rate and polymer molecular weight. A model implementing a living kinetic scheme is first developed and validated by comparison with the experimental results. The rate coefficients of the main reactions (activation, propagation, and reversible chain transfer) have been evaluated. Finally, to predict with accuracy the broadening of the molecular weight distribution, we introduce ester interchange reactions, so-called "transesterifications", into the kinetic scheme, and the corresponding rate coefficient is evaluated.

Introduction

As a substitute of petroleum-based polymers, biodegradable polymers are currently attracting a lot of interest because of their biocompatible, biodegradable properties. Their properties make the polymers suitable for many different applications, such as packaging, drug delivery, and tissue engineering.[1−4] Homo-poly(lactic acid) (PLA) and its copolymers are especially promising because of their excellent physical properties.[5,6] PLA can be produced mainly by two routes, direct polycondensation[7−9] and ring-opening polymerization (ROP).[10−13] For large-scale applications, the ROP route indeed attracts high interest from industry, and a such reaction step is actually involved in commercial processes.[14−16]

The synthesis of PLA by ROP was first reported by Carothers et al.[9] in 1932. Low-molecular-weight polymer was produced, and the synthesis of high-molecular-weight materials was not possible until the development of effective lactide purification techniques in 1955.[11,12] During the last half century, many different catalysts have been studied to increase the reaction productivity; they have been recently reviewed by Upadhyay et al.[17] Among them, 2-ethylhexanoic acid tin(II) salt ($Sn(Oct)_2$) is the most widely used in both scientific research and industrial production and is the only catalyst that has been accepted by the U.S. Food and Drug Administration.[1]

The mechanism of ROP of lactide catalyzed by $Sn(Oct)_2$ has been investigated by many researchers. On the basis of the extensive set of experimental data available in the literature, almost all of the possible mechanisms were proposed during the last 30 years involving multiple different steps, such as initiation, propagation, and chain transfer to low-molecular-weight species and to polymer.[18] The key step of initiation was especially debated: notably, all proposed mechanisms involve the contributions of OH-bearing species, such as water, alcohols, or carboxylic acids. A comprehensive presentation of all possible mechanisms is available in the review by Duda and Penczek.[19] In this work, we just provide a short account of the two most popular rival initiation mechanisms: the first mechanism (mainly from Kricheldorf et al.[20,21]) is based on a kind of "monomer activation", where monomer, OH-bearing species, and catalyst form a ternary complex. Accordingly, Sn atoms are not bonded to the active chains, and the corresponding polymerization rate is simply first order with respect to the initial amounts of catalyst and alcohol. The second one was proposed by Penczek et al.[18] and is based on the "alkoxide initiation mechanism". Accordingly, Stannous Octoate actually reacts with OH-bearing species to form an alkoxide that is the species initiating the polymerization. Therefore, $Sn(Oct)_2$ and OH groups are initiator and coinitiator, respectively, often indicated as catalyst and cocatalyst. The direct observation of macromolecules containing Oct−Sn−O− end groups by MALDI-TOF and the dependences of the polymerization rate upon monomer, catalyst, and cocatalyst concentrations are solid evidence in favor of this mechanism.[19] Moreover, the same authors proposed a comprehensive kinetic scheme of the reaction, also involving reversible chain transfer and polymer interchange reactions, so-called "transesterifications"; such reactions are responsible for the fast interchange of active end groups among the polymer chains and directly affect the molecular weight distribution of the final polymer. The resulting polymerization mechanism is currently the most accepted, and it will be used in the model developed in this article.

In contrast with such a huge body of experimental work, only a few publications focus on mathematical modeling of such polymerization or at least on the evaluation of the corresponding rate coefficients. The first systematic kinetic analysis of ROP for PLA synthesis catalyzed by $Sn(Oct)_2$ was reported by Eenink.[22] After his work, the influence of different process parameters on the polymer characteristics was elucidated. The corresponding "apparent" propagation rate coefficient, k_{eff} (defined as the pseudo-first-order propagation rate coefficient with respect to monomer, $k_{eff} = k_p R^*$, where R^* is the concentration of active chains and k_p is the propagation rate coefficient) was evaluated. However, the role of "natural" or environmental impurities, such as moisture and acidic species, on reaction behavior was not considered at all. In contrast, Zhang et al.[23] found that hydroxyl

*Corresponding author. E-mail: massimo.morbidelli@ghem.ethz.ch.

Published on Web 10/12/2009

and carboxylic acids strongly affect the reaction rate. Later on, Witzke et al.[24] reported a more comprehensive kinetic scheme of ROP of lactide in bulk. They introduced a "semiliving" behavior, meaning that transesterification reactions are active along with reversible propagation. The values of the Arrhenius parameters for both reactions, propagation and transesterification, were reported.[25] More recently, Puaux et al.[26] and Mehta et al.[27,28] developed models based on the cationic mechanism;[29] accordingly, the kinetic scheme involved irreversible initiation, irreversible propagation, and irreversible chain transfer to monomer and impurities. By suitable parameter fitting, such models exhibit good agreement in terms of conversion and number-average molecular weight (M_n), even though the broadening of the molecular weight distribution is always largely underestimated.

Aimed to fill the gap between the experimental and the modeling efforts still present in the literature, this work is reporting the development of a model based on the alkoxide initiation mechanism. A new set of experimental data of bulk melt ROP of L,L-lactide with $Sn(Oct)_2$ as catalyst and 1-dodecanol as cocatalyst has been collected. Reactions at different values of the molar ratios between monomer and catalyst and between catalyst and cocatalyst are examined. Conversion and average molecular weights are measured in time. Such data are combined with a suitable model based on the alkoxide initiation mechanism and accounting for transesterification reaction. The values of all rate coefficients appearing in the kinetic scheme have been evaluated, mostly using a simplified analysis of the data and partially by direct fitting of the model predictions to the experimental results.

Experimental Part

Materials. (*S*,*S*)-3,6-Dimethyl-1,4-dioxane-2,5-dione (L,L-lactide; Sigma Aldrich, 98% purity) was further recrystallized in extra dried puriss. Toluene (Riedel-de Haën, purity ≥99.7%, H_2O content <0.001%), 2-ethylhexanoic acid tin(II) salt ($Sn(Oct)_2$, Sigma Aldrich, 95% purity), and 1-dodecanol (ROH, Fluka, 99.5% purity) were used as received. For SEC analyses, polystyrene standards from 500 to 2 000 000 Da (Sigma Aldrich) were used for calibration, and chloroform (J. T. Baker) was used as eluent. Hydranal-Coulomat (Riedel-de Haën) was used as Karl Fischer (KF) reagent. Extra dried puriss. acetonitrile (Fluka, purity ≥99.5%, H_2O content <0.001%) was used as solvent during KF titrations. Sodium ethoxide (Acros Organics, 96% purity), ethanol (Merck, 99.9% purity), potassium phthalate monobasic (Fluka, purity ≥99.5%), and bromothymol blue (Fluka, Technical grade) were used for titration.

Reaction Procedure. L,L-Lactide (LA) was first dried overnight at 30 °C under vacuum after recrystallization in toluene. It was melted at temperature <100 °C in a stirred flask in glovebox; then, $Sn(Oct)_2$ and ROH were prepared in glovebox at a given molar ratio with respect to monomer in toluene (10 wt %). Anhydrous toluene was used to facilitate the transfer of catalyst and cocatalyst to the reaction vessels without contaminations. Namely, such mixtures were transferred to glass vials and sealed with T-type poly(tetrafluoroethylene) caps to prevent the loss of LA during the reaction by vaporization and recrystallization. All vials were finally transferred into a controlled heating block set at temperature of 130 ± 1 °C. PLA products in the different reaction vials were finally quenched in an ice bath at different times and kept for further characterizations. Reactions at constant amount of catalyst and different ratios catalyst/cocatalyst have been carried out as well as reactions at different catalyst amounts and constant ratio catalyst/cocatalyst.

Size Exclusion Chromatography Analysis. Conversion and molecular weight distribution of all samples were characterized by size exclusion chromatography (SEC) (Agilent, 1100 series) equipped with two detectors, ultraviolet (UV) and differential refractive index (RI). Depending on the molecular weight of the specific sample, a precolumn with an oligopore column (Polymer Laboratories, length of 300 mm and diameter of 7.5 mm, measuring range: 0−4500 Da) or a pre-column with two PLgel 5 μm MIXED-C columns (Polymer Laboratories, length of 300 mm and diameter of 7.5 mm, measuring range: 2000−2 000 000 Da) have been used. Chloroform was used as eluent at flow rate of 1 mL min^{-1} and temperature of 30 °C. Universal calibration was applied, based on poly(styrene) standards and the following equation[30]

$$\ln M_2 = \frac{1+a_1}{1+a_2} \ln M_1 + \frac{1}{1+a_2} \ln\left(\frac{K_1}{K_2}\right) \quad (1)$$

where a and K are the Mark−Houwink constants for PLA (index 2) and the reference polymer (index 1). The effective use of the universal calibration asks for reliable values of such constants for both polymers. For PLA, many values are available in the literature from different sources (cf. refs 31 and 32). Such values are quite scattered, and the selection of the most reliable ones is not easy; moreover, different values are also reported for different PLA stereo configurations. Luckily enough, the topic was recently revisited by Dorgan et al.[33] in a very comprehensive way. Namely, they studied the relationship between viscosity and molecular weight by using different characterization techniques such as viscometry, SEC, static multiangle light scattering (SLS), ellipsometry, and rheometry. The best values of Mark−Houwink constants for PLLA, the specific configuration under examination here, were determined at 30 °C in chloroform. Values inside the ranges reported in such a paper ($K = 0.01709$ mL g^{-1} and $a = 0.806$) are used in this work along with the following values for poly(styrene): $K = 0.0049$ mL g^{-1} and $a = 0.794$.[34]

Karl Fischer Titration. Water contents of all reagents were analyzed by 831 KF coulometer (Metrohm). Toluene and 1-dodecanol (in bulk) were measured directly by KF titration. LA was dissolved in extra-dry acetonitrile. Round−Robin tests for determining water contents by KF titration were carried out. All solutions were prepared in glovebox (2−10 ppm).

The water contents in extra dried toluene and 1-dodecanol are 24 and 148 ppm respectively. Considering the molar ratio with respect to the monomer, they are negligible. The water content of LA ranges from 20 to 100 ppm, which has to be counted during simulation of models. The water content of 2-ethylhexanoic acid tin(II) salt cannot be determined by Karl Fischer measurement because the stannous tin will react with Karl Fischer reagent to yield a false high water content.

Nonaqueous Titration. To determine the amount of acidic impurities in both crude and purified LA, we carried out nonaqueous titrations by using Dosimat 665 and Titroprocessor 686 (Metrohm) with nonaqueous electrode (catalogue no.: 6.0229.100). Sodium ethoxide ethanol solution was used as titrant and calibrated by potassium phthalate monobasic standard. Crude and purified LA ethanol solutions with bromothymol blue as indicator were titrated; the final results were subtracted by the background, as determined from the blank titration (Table 1).

Table 1. Analysis of Acidic Impurities by Nonaqueous Titration

	concentration	acid residue [meq kg^{-1}]
ethanol puriss.	bulk	0.041
crude L,L-lactide	25 g L^{-1}	30.55
purified L,L-lactide	25 g L^{-1}	0.242

Experimental Results

As anticipated, the temperature of all reactions was constant and equal to 130 °C: such value is generally below the melting temperature of PLA, ranging from 135 to 180 °C depending upon the molecular weight.[35−39] Therefore, polymer phase separation is expected under the operating conditions. Also, the kinetics of such a phase change has to be considered: the characteristic time

of crystallization is usually quite large, ranging from 20 to 60 min in the absence of reaction,[40−42] and such time increases at increasing chain length. To check the actual presence of polymer solidification, the physical state of the samples collected during a slow reaction producing high molecular weight was visually controlled; no signal of solidification was noticed during the first 3 h, thus indicating that the characteristic time of phase change is much longer than that of reaction. Accordingly, because the modeling analysis reported below is focused on the first 1 to 1.5 h of reaction, the role of polymer solidification and crystallization is completely neglected in the rest of the discussion, and the reaction is presumed to take place in a single liquid phase.

ROPs are often exhibiting living behavior; that is, the reaction proceeds at a constant number of growing chains.[43,44] For a living system with reversible propagation and reversible deactivation, the following well-known relationships apply

$$Y = \ln\left[\frac{(M_0 - M_{eq})}{(M - M_{eq})}\right] = k_p R^* t \quad (2)$$

$$M_n = \frac{M_0 X}{R^* + D} M_m \quad (3)$$

where R^* is the concentration of living chains, D is that of dormant (reversibly terminated) chains, X is monomer conversion, defined as $(M_0 - M)/M_0$, where M is the monomer concentration and M_0 is the initial monomer concentration, M_m is the molecular weight of monomer, and Y is the logarithm of the normalized conversion defined as in eq 2. Note that such relationships apply when irreversible terminations are absent. Moreover, if propagation and reversible deactivations are only operative, then narrow molecular weight distributions are obtained, that is, with dispersity values ($P_d = M_w/M_n = (\lambda_0+\mu_0)(\lambda_2+\mu_2)/(\lambda_1+\mu_1)^2$, where λ_n is the nth order moment of living chains and μ_n is the nth order moment of dormant chains) very close to one. Finally, if the quantities Y and M_n exhibit linear behavior with time and conversion, respectively, then the concentrations of active and dormant chains are constant all along the reaction.

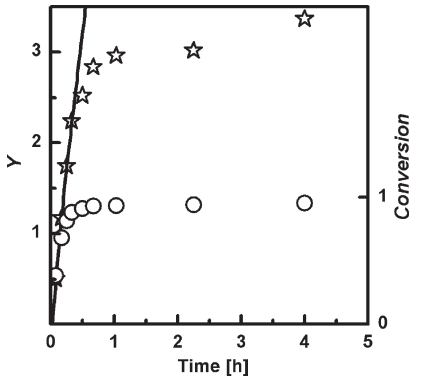

Figure 1. Kinetics of LA polymerization at M/C = 3771 and ROH/C = 5. Symbols: ○, conversion; ☆, Y (cf. eq 2).

To check the livingness of the reacting system at constant temperature, Y and M_n have been plotted versus time (t) and conversion, respectively. The result of this check is first shown in Figure 1 in terms of conversion for a specific reaction. Even though the evolution of the monomer conversion is clearly nonlinear in time, the quantity Y is linear, at least at conversion values <95%. This means that the concentration of the active chains is constant during most of the reaction and for sure up to conversion >90%. At higher conversion, that is, at very long reaction time, the concentration of active chains decreases and the reaction is not living any longer. Such behavior has been previously reported by other researchers;[25,29,45] even though the specific mechanisms determining such behavior (irreversible termination reactions effective at high conversion, polymer crystallization) are not clear, such loss of livingness is a fact. Because our aim here is to catch the major kinetic phenomena of the reaction, we confine ourselves to the living part of the reaction, that is, to conversion values up to 90% or, in terms of reaction time, to no more than 1 to 1.5 h.

Keeping in mind this limitation, livingness is checked for all reactions at different ratios ROH/C in Figure 2a, where C represents the catalyst, $Sn(Oct)_2$. A convincing linearity is established in all cases, thus confirming the living nature of the ROP under examination at least for conversion <90%. Another interesting feature clearly shown in the same Figure is the effect of the increasing ratio ROH/C; starting from the reaction at ROH/C = 1, the polymerization rate increases first but levels off above a certain amount of ROH. The corresponding values of the apparent propagation rate coefficient, k_{eff}, are plotted versus ROH/C in Figure 2b as well. For values of the ratio alcohol/catalyst >20, the different Y lines are fully superimposed, and a clear plateau is established in Figure 2b, thus indicating that larger amounts of alcohol do not affect the reaction rate anymore. This behavior strongly supports a catalyst activation mechanism by reaction with the alcohol, as proposed in the literature;[18] such reaction is complete when the ratio OH/C is >20, and the addition of more alcohol becomes ineffective from the activation viewpoint.

Let us now examine the molecular weight behavior. The number-average molecular weights (M_n) shown in Figure 3 versus conversion exhibit nice linearity in all cases: according to eq 3, this is also proof of the livingness of the reaction and of the constant concentration of the polymer chains, active and dormant. Ideal living conditions are somehow lost during the

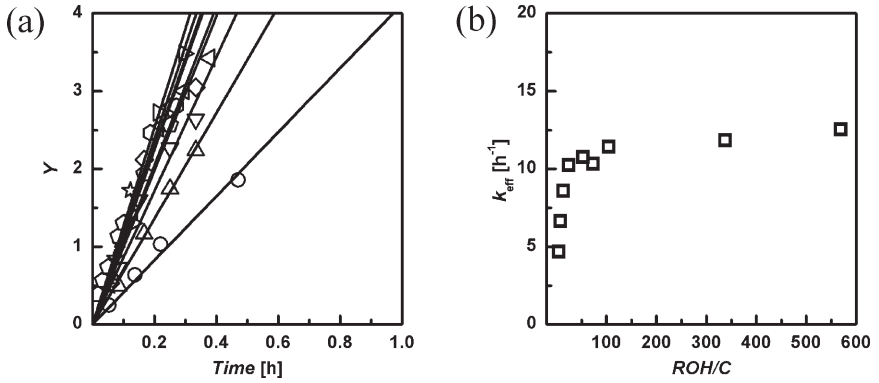

Figure 2. (a) Kinetics of LA polymerization and (b) apparent propagation rate coefficient at M/C = 3771 and different ratios ROH/C: ○, 1; △, 5; ▽, 10; ◇, 20; left tilted open triangle, 50; right tilted open triangle, 70; open hexagon, 100; ☆, 335; open pentagon, 565.

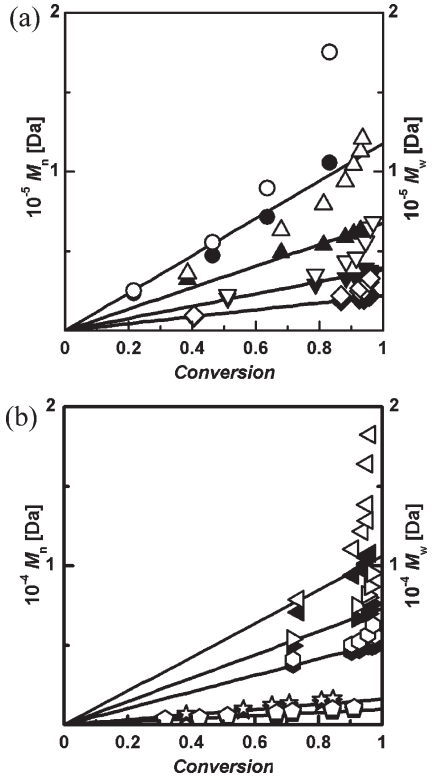

Figure 3. M_n (full symbols) and M_w (empty symbols) of PLA at constant M/C = 3771 and different ROH/C values: (a) ○ ●, 1; ▲ △, 5; ▼ ▽, 10; ◆ ◇, 20; solid left tilted triangle and open left tilted triangle, 50, solid right tilted triangle and open right tilted triangle, 70; solid hexagon and open hexagon, 100; ★ ☆, 335; open pentagon and solid pentagon, 565. Solid lines evaluated by linear fitting.

reaction, as indicated by the increasing discrepancy between the M_n and M_w values. The clear divergence of the dispersity of the molecular weight distribution from unity proves that side reactions are operative which do not affect the total number of chains but only their length.

Taking advantage of the linear behavior of M_n, we can calculate the molar concentration of polymer chains (active and dormant) from eq 3. Such evaluation was carried out for all reactions at constant catalyst concentration, and the results are summarized in Table 2, where N_c ($N_c = R^* + D$) indicates the total molar concentration of chains. If we compare the estimated values to the initial alcohol concentration according to the recipe, then they are very close, thus proving the key role of alcohol in both activation and reversible deactivation. The estimated values of N_c are systematically larger than the amounts of alcohol introduced, with 7.9×10^{-3} mol L^{-1}. This discrepancy can be explained as additional chain initiation because of "environmental impurities" (any OH-bearing species, such as water from air or from $Sn(Oct)_2$ itself). Whatever the source of such environmental impurities, their amount will be accounted for in the model simulations discussed in the following. Namely, all experimental results will be presented in the rest of the article in terms of "nominal" ROH/C ratios, that is, those corresponding to the recipe. However, the "actual" values of such ratio given by $(ROH/C)_{actual} = ((ROH + \Delta)/C)$ (i.e., corrected using the average value of the concentration of environmental impurities as estimated from Table 2) have been considered when simulating these experiments by the model presented below.

It is worth noticing that the environmental impurities, including water and acid species, would play a major role on kinetics and molecular weight in experiments without cocatalyst (ROH/C = 0). Because the environmental impurities are difficult to be kept under control experimentally, such a condition has not been studied in this article, and 1-dodecanol was always used as cocatalyst at ROH/C ≥ 1.

Table 2. Estimated Values of Moles of Polymer Chains for Reactions at Constant Catalyst Amount and Different ROH/C Values

ROH/C	N_c (mol L^{-1})	ROH_0 (mol L^{-1})	$N_c - ROH_0$ (mol L^{-1})
565	1.22	1.21	8.98×10^{-3}
335	7.22×10^{-1}	7.16×10^{-1}	5.62×10^{-3}
100	2.24×10^{-1}	2.14×10^{-1}	1.03×10^{-2}
70	1.56×10^{-1}	1.50×10^{-1}	6.67×10^{-3}
50	1.14×10^{-1}	1.07×10^{-1}	6.98×10^{-3}
20	5.28×10^{-2}	4.28×10^{-2}	1.00×10^{-2}
10	3.01×10^{-2}	2.14×10^{-2}	8.77×10^{-3}
5	1.66×10^{-2}	1.07×10^{-2}	5.87×10^{-3}
1	9.87×10^{-3}	2.14×10^{-3}	7.73×10^{-3}

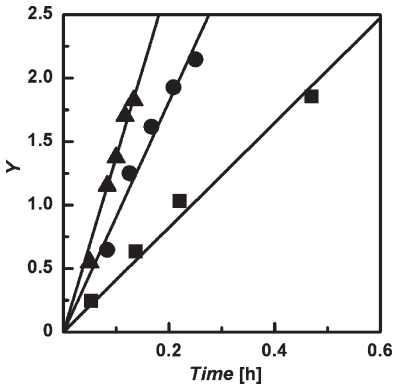

Figure 4. Kinetics of LA polymerization at ROH/C = 1 and different values of the ratio M/C: ■, 3771; ●, 1000; ▲, 500.

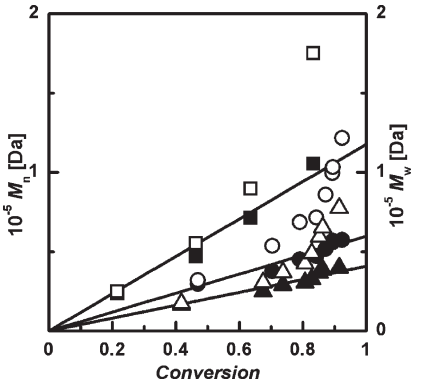

Figure 5. M_n (full symbols) and M_w (empty symbols) versus conversion at constant ROH/C = 1 and different values of the ratio M/C: ■, 3771; ●, 1000; ▲, 500.

Finally, another set of experiments at different catalyst amounts and constant ROH/C ratio was carried out. The same check of livingness discussed above was applied, and the results are summarized in Figures 4 and 5 and Table 3. In particular, the concentration of environmental impurities is a clear function of the catalyst amount. Because the unknown impurities in the catalyst could not be measured with accuracy, the actual amount of impurities as reported in Table 3 will be applied in the corresponding model simulations reported later in this work.

The same arguments discussed for the reactions at different amounts of alcohol also apply in this case. As expected, by increasing the amount of catalyst at constant equimolar ratio with alcohol, the reaction rate increased, again indicating the activation interplay between the two species. M_n decreased because of the increasing number of living and total chains corresponding to the increasing amount of catalyst and cocatalyst, respectively.

Table 3. Estimated Values of Moles of Polymer Chains for Reactions at ROH/C = 1 and Different M/C Values

M/C	N_c (mol L^{-1})	ROH_0 (mol L^{-1})	$N_c - ROH_0$ (mol L^{-1})
3771	9.87×10^{-3}	2.14×10^{-3}	7.73×10^{-3}
1000	1.94×10^{-2}	8.06×10^{-3}	1.14×10^{-2}
500	3.01×10^{-2}	1.61×10^{-2}	1.40×10^{-2}

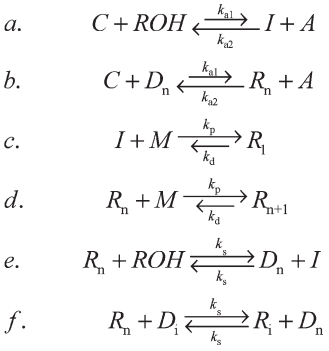

Figure 6. Simplified kinetic scheme for ROP of PLA with $Sn(Oct)_2$ as the catalyst and an alcohol as the cocatalyst, ROH.

Kinetic Scheme and Preliminary Analysis

On the basis of the experimental results reported in the previous section and the literature analysis summarized above, the kinetic scheme in Figure 6 is proposed. It is a reduced version of the general one proposed by Penczek et al.[18] and already mentioned in the Introduction.

Basically, three types of reversible reactions can be identified: activations, propagations, and reversible deactivations. Reaction *a* is catalyst activation by alcohol, forming the truly active species −SnOR and octanoic acid, indicated by *I* and *A*, respectively. Note that each molecule of catalyst produces two active groups; therefore, the concentration of *C* should be twice the experimental concentration of the catalyst, $Sn(Oct)_2$. Even though reaction *a* involves ROH, all OH-bearing species are able to reversibly activate the catalyst to form the active alkoxide groups. Accordingly, reaction *b* is also introduced: this is the reaction between the catalyst and a dormant chain *D*, the species indicated as HO−$(LA)_n$−H in the general scheme in ref 18. Because of the similarity between the two reactions, the same rate coefficients are used just to keep the number of parameters in the final model as small as possible. Finally, it should be mentioned that according to the literature,[18] the activation rate should be slower than deactivation; therefore, the value of the corresponding equilibrium constant, $K_{eq,a} = k_{al}/k_{a2}$, is expected to be smaller than one.

Third and fourth reactions, *c* and *d*, are the reversible propagation steps, those affecting the length of the active (or living) chains, R_n. The values of the corresponding rate coefficients are assumed to be independent of the chain length and applicable to both reactions. The corresponding equilibrium coefficient, $K_{eq,p} = k_p/k_d$, where k_d is the depropagation rate coefficient, is readily estimated given the maximum achievable conversion.

The last two reactions, *e* and *f*, are actually reversible chain transfer reactions. Let us focus on the first one: the reaction between an active chain and a molecule of alcohol results in a dormant chain with the same length and a new alkoxide group, which starts growing by the propagation reaction *c*. Because this transfer reaction is reversible, it is not affecting the system reactivity (the number of active chains remains the same) but strongly affects the molecular weight, that is, the total number of chains, N_c. Reaction *f* is a completely equivalent transfer involving a dormant chain as the OH-bearing species; such reaction is not given in the original kinetic scheme by Penczek et al.[18] because it does not affect the concentration of both active and dormant species. However, this reaction is accounted for in the model reported below to predict the evolution of the molecular weight reliably. Once more, the same rate coefficients are considered for both reactions *e* and *f*; moreover, because of the complete equivalence of the reaction in both directions in the case of f, the same values are expected for both forward and backward reactions, which means the corresponding equilibrium constant $K_{eq,s} = 1$, as also suggested in ref 18.

With reference to the simplified kinetic scheme in Figure 6, it is now useful to write down the corresponding set of material and population balances with reference to a well-stirred, homogeneous batch reactor

$$\frac{dC}{dt} = -k_{a1}CROH + k_{a2}IA - k_{a1}C\sum_{n=1}^{\infty} D_n + k_{a2}\sum_{n=1}^{\infty} R_n A \quad (4)$$

$$\frac{dA}{dt} = k_{a1}CROH - k_{a2}IA + k_{a1}C\sum_{n=1}^{\infty} D_n - k_{a2}\sum_{n=1}^{\infty} R_n A \quad (5)$$

$$\frac{dROH}{dt} = -k_{a1}CROH + k_{a2}IA - k_s ROH\sum_{n=1}^{\infty} R_n + k_s I\sum_{n=1}^{\infty} D_n \quad (6)$$

$$\frac{dI}{dt} = -k_p MI + k_d R_1 + k_{a1}CROH - k_{a2}IA + k_s ROH\sum_{n=1}^{\infty} R_n - k_s\sum_{n=1}^{\infty} D_n I \quad (7)$$

$$\frac{dR_1}{dt} = k_p MI - k_p MR_1 + k_d R_2 - k_d R_1 + k_{a1}D_1 C - k_{a2}R_1 A - k_s R_1 ROH + k_s D_1 I - k_s R_1\sum_{n=1}^{\infty} D_n + k_s D_1\sum_{n=1}^{\infty} R_n \quad (8)$$

$$\frac{dR_n}{dt} = k_p R_{n-1}M - k_p R_n M + k_d R_{n+1} - k_d R_n + k_{a1}D_n C - k_{a2}R_n A - k_s R_n ROH + k_s D_n I - k_s R_n\sum_{i=1}^{\infty} D_i + k_s D_n\sum_{i=1}^{\infty} R_i \quad n \geq 2 \quad (9)$$

$$\frac{dD_n}{dt} = -k_{a1}D_n C + k_{a2}R_n A + k_s R_n ROH - k_s D_n I + k_s R_n\sum_{i=1}^{\infty} D_i - k_s D_n\sum_{i=1}^{\infty} R_i \quad (10)$$

$$\frac{dM}{dt} = -k_p MI - k_p M\sum_{n=1}^{\infty} R_n + k_d\sum_{n=1}^{\infty} R_n \quad (11)$$

The previous set of equations can be greatly simplified by summing up the balances of all active (eqs 8 and 9) and

dormant (eq 10) chains. The following lumped balances are obtained

$$\frac{dC}{dt} = -k_{a1}C(ROH + D) + k_{a2}A(I + R) \quad (12)$$

$$\frac{dA}{dt} = -\frac{dC}{dt} \quad (13)$$

$$\frac{dROH}{dt} = -k_{a1}C\,ROH + k_{a2}IA - k_s R\,ROH + k_s ID \quad (14)$$

$$\frac{dI}{dt} = -k_p MI + k_d R_1 + k_{a1}C\,ROH - k_{a2}IA + k_s R\,ROH - k_s DI \quad (15)$$

$$\frac{dR}{dt} = k_p MI - k_d R_1 + k_{a1}DC - k_{a2}RA - k_s R\,ROH + k_s DI \quad (16)$$

$$\frac{dD}{dt} = k_s R\,ROH - k_s DI - k_{a1}DC + k_{a2}RA \quad (17)$$

$$\frac{dM}{dt} = -k_p MI - k_p MR + k_d R \quad (18)$$

where R and D indicate the total concentrations of active and dormant chains of any length, respectively, defined as $R = \sum_{n=1}^{\infty} R_n$ and $D = \sum_{n=1}^{\infty} D_n$. The last set of equations can be further reduced by focusing on the total concentrations of active and OH-bearing species, that is, $R^* = I + R$ and $OH = ROH + D$. The corresponding balances are readily obtained by summing eqs 15 and 16 and 14 and 17

$$\frac{dR^*}{dt} = k_{a1}C\,OH - k_{a2}R^*A \quad (19)$$

$$\frac{dOH}{dt} = -k_{a1}C\,OH + k_{a2}R^*A \quad (20)$$

By inspection of the final version of the material balances (eqs 12, 13, 19, and 20) the following differential constraints are readily shown to apply

$$dR^* = -dOH = -dC = dA \quad (21)$$

By integrating eqs 21, the amounts of the different species at any time are related to the initial values (indicated by the subscript 0; initial zero values of active species and acid are obviously assumed) as follows

$$R^* = OH_0 - OH = C_0 - C = A \quad (22)$$

It is worth noticing that these relationships apply all along the process, from the beginning to the end; therefore, given the time evolution of a reference variable, for example, the catalyst concentration, C, the total concentrations of all the other species, active (R^*), OH-bearing (OH), and acid (A), are readily evaluated.

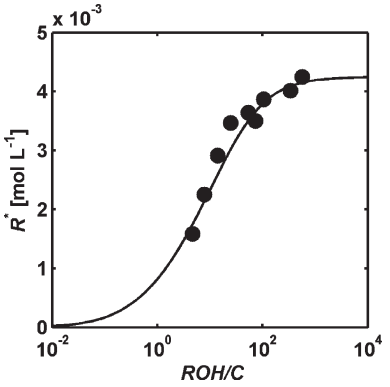

Figure 7. Comparison between estimated (symbols) and calculated (eq 24) values of R^* at different values of the ratio ROH/C.

Let us now come back to the experimental results Y versus time (Figures 1, 2, and 4) and M_n versus conversion (Figures 3 and 5); the linear behavior is achieved in both cases very early in time, just after the reaction starts. According to eqs 1 and 2, this behavior indicates that constant values of active and dormant species are quickly established, thus suggesting fast equilibration of the activation and the reversible termination reactions. Therefore, assuming equilibrium conditions for activation reactions, the time derivatives in eqs 19 and 20 are equal to zero, and the following algebraic relationship is obtained

$$\frac{R^*A}{C\,OH} = \frac{k_{a1}}{k_{a2}} \equiv K_{eq,a} \quad (23)$$

which is the conventional expression of the reaction equilibrium constant in terms of concentrations. Combining this equation with the equalities (eq 22), a quadratic formula expressing the catalyst concentration, C, as a function of the initial concentrations and of the activation equilibrium constant is obtained, of which the analytical solution is

$$C = \frac{2C_0 + K_{eq,a}(OH_0 + C_0) - \sqrt{[2C_0 + K_{eq,a}(OH_0 + C_0)]^2 - 4C_0^2(1 - K_{eq,a})}}{2(1 - K_{eq,a})} \quad (24)$$

In summary, under the assumption of instantaneous equilibrium for activation, the analytical solution of the last previous equation provides the final concentration of residual catalyst, from which the corresponding concentrations of OH-bearing species, active species, and octanoic acid are readily obtained from eq 22. Notably, according to eq 24, the equilibrium concentration of the catalyst is equal to the initial value and approaches zero at zero alcohol and $OH_0 \gg C_0$, respectively.

Let us now fully exploit the main results of the previous analysis (instantaneous activation based on OH-bearing species). By inspection of the data in Figure 2b, the concentration of active species, R^*, can be assumed to be equal to the initial amount of catalyst at large values of the ratio ROH/C. Accordingly, being the product of the propagation rate coefficient and R^* equal to the plateau value of k_{eff} versus time at the largest values of the ratio, the corresponding value of k_p is readily estimated (2952 L mol^{-1} h^{-1}). We compared this value with the available literature: because most literature sources provide k_{eff} only (thus preventing any fair comparison), we selected the values reported in refs 18 and 19 for solution polymerization at lower temperatures (50 and 80 °C). Using the value of activation energy of 70.9 kJ/mol reported by ref 25, k_p values from 2030 to 7670 L mol^{-1} h^{-1} are estimated, thus confirming the reliability of our value.

Table 4. Numerical Values of Some Model Parameters

parameter	symbol	value	source
activation equilibrium constant	$K_{eq,a}$	0.15	this work
chain transfer equilibrium constant	$K_{eq,s}$	1	ref 18
propagation rate coefficient	k_p	2952 L mol^{-1} h^{-1}	this work
monomer equilibrium concentration	M_{eq}	0.106 mol L^{-1}	ref 25

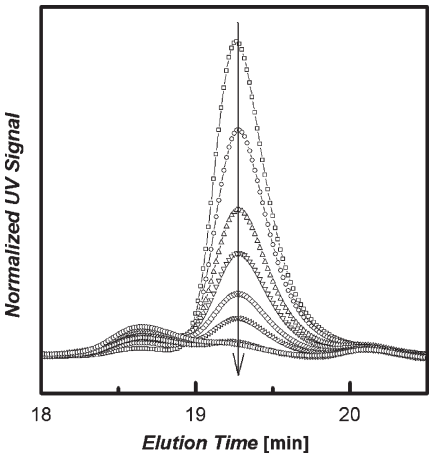

Figure 8. SEC chromatograms of monomer peaks at different conversion at M/C = 3771 and OH/C = 10 (arrow indicating increasing conversion).

Furthermore, by using such value of k_p, the total concentration of living chains R^* at each different amount of ROH can also be estimated: the resulting values are shown in Figure 7. By fitting eq 24 to such values, the activation equilibrium constant has been estimated to be $K_{eq,a} = 0.15$. (Note that the values of the ratio ROH/C in the Figure have been adjusted to account for the environmental impurities as explained in the previous section, that is, introducing a constant, average amount of additional alcohol equals to 7.9×10^{-3} mol L^{-1}.)

Model Development: Activation, Propagation, and Reversible Chain Transfer

Let us now come back to the complete set of material and population balances as given by eqs 4−11. Exactly those equations have been numerically solved using the method of moments for the population balances; the final moment equations are reported in the Appendix. Moreover, the selected values of the equilibrium constants of all reactions, along with the rate coefficient of propagation, are listed in Table 4.

The values of both the propagation rate coefficient and the activation/chain transfer equilibrium constants are those determined as detailed in the previous section.

The monomer equilibrium concentration (M_{eq}), defined as k_d/k_p and equal to the reciprocal of the more conventional equilibrium constant of the reaction, was found in the literature at 130 °C;[24] such value is consistent with a value of equilibrium conversion of 98.7%. Actually, the average value of the equilibrium conversion we estimated from our experiments was slightly smaller and equal to 96.5%, corresponding to an M_{eq} value of 0.106 mol L^{-1}. The reason for such discrepancy is most probably due to the limited accuracy of our experimental evaluation of the residual monomer amount by SEC. This is better understood by looking at the SEC chromatograms in Figure 8, where the collected UV signals for a typical reaction are shown as a function of the reaction time in the region of the low-molecular-weight species. Whereas the monomer peak (elution time around 19.3 min) is clearly decreasing with conversion, a second peak at shorter elution time (around 18.7 min, i.e., larger molecular weight) is appearing at high conversions. Because of the minor relevance of such peak, its area was arbitrarily attributed to the monomer, and thus the corresponding residual monomer amount was overestimated. Therefore, the M_{eq} value from the literature should be more reliable, and it has been used in all model simulations.

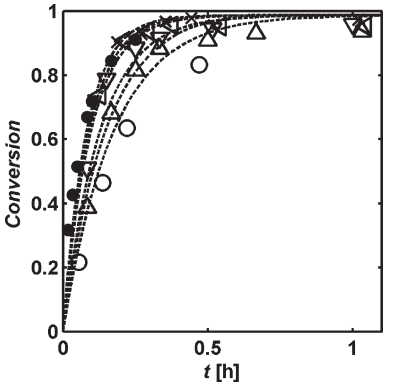

Figure 9. Conversion versus time for LA polymerization with Sn(Oct)$_2$ and ROH. M/C = 3771, different ROH/C values. Experimental data: ○, 1; △, 5; ▽, 10; left tilted open triangle, 50; ×, 100; ●, 565; model results, dashed lines.

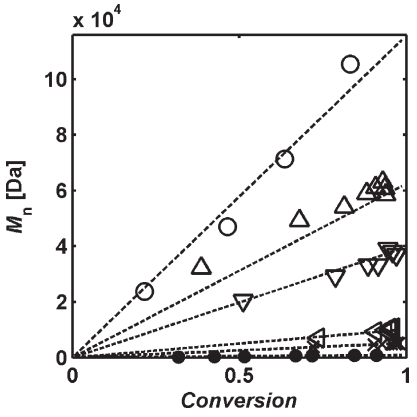

Figure 10. M_n versus conversion for LA polymerization with Sn(Oct)$_2$ and ROH. M/C = 3771, different ROH/C values. Experimental data: ○, 1; △, 5; ▽, 10; left tilted open triangle, 50; ×, 100; ●, =565; model results, dashed lines.

Finally, very large values of the rate coefficients of both activation and transfer reactions have been assumed ($k_{a1} = k_s = 10^6$ L mol^{-1} h^{-1}) to achieve complete equilibration in very short time, as indicated by experiments. Of course, the rate coefficients of the corresponding inverse reactions are consistent with the equilibrium constants in Table 4. Such values are just large enough to produce an almost instantaneous approach to equilibrium conditions: actually, any value larger than 10^6 L mol^{-1} h^{-1} can be used without significant effects on the model predictions. It should be made clear that following the preliminary analysis of the previous section, no parameter adjustment has been applied when running this version of the model.

The comparisons between experimental results and model predictions are shown in Figures 9−12 for the experiments at different OH/C ratios. The predictions of conversion and number-average molecular weight evolutions are quite satisfactory. This is not surprising because it is fully consistent with the preliminary analysis.

Discrepancies appear in terms of weight-average molecular weights (M_w) (Figure 11); they are quite evident as a function of

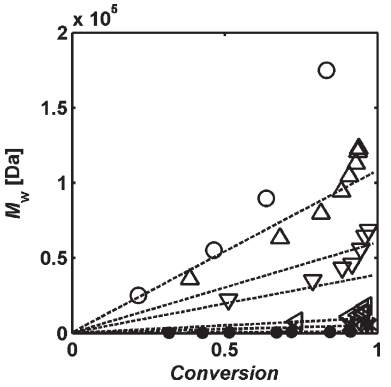

Figure 11. M_w versus conversion for LA polymerization with $Sn(Oct)_2$ and ROH. M/C = 3771, different ROH/C values. Experimental data: ○, 1; △, 5; ▽, 10; left tilted open triangle, 50; ×, 100; ●, 565; model results, dashed lines.

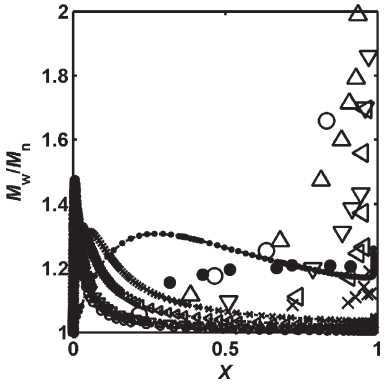

Figure 12. Dispersity versus conversion for LA polymerization with $Sn(Oct)_2$ and ROH. M/C = 3771, different ROH/C values. Experimental data: ○, 1; △, 5; ▽, 10; left tilted open triangle, 50; ×, 100; ●, 565; model results, dashed lines.

conversion, where an increase in the experimental values with respect to the model predictions is exhibited at conversion values larger than about 50−60%. Such discrepancies become even more explicit in terms of dispersity, M_w/M_n. These results prove that the simplified kinetic scheme in Figure 6 is not accounting for all reactions actually taking place. Because the reactions kinetics (polymerization rate, numbers of active and total chains) are correctly predicted by this version of the model, the missing reactions should not affect those quantities but only the "shape" of the molecular weight distribution.

Model Development: Transesterification Reactions

Side reactions often mentioned as affecting the molecular weight of polyesters are the molecular interchanges, so-called "transesterifications". Different interchange reactions are possible, such as inter- and intratransesterification; however, it has been reported that inter-transesterification is the dominant mechanism in the bulk catalyzed ROP of lactide at 130 °C.[46−50]

The corresponding reaction scheme is shown in Figure 13: the reactions are fully reversible, and the catalytic site is responsible for the chain scission step. Whereas the reaction between two active chains (the first one in the Figure) is the one previously mentioned in the literature (cf. refs 19 and 49), the reaction involving the dormant chains is original. Because of the large amount of dormant chains present in the system at large ROH concentrations, we believe it has to be accounted for in any model aimed to evaluate the molecular weight of the polymer. Following the clear schematization reported in ref 49, in both cases, an active

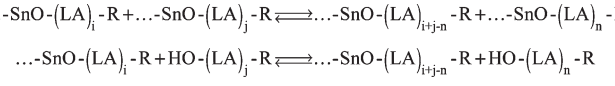

Figure 13. Reaction mechanism of transesterification.

chain end is "attacking" an ester bond internal to another chain, active or dormant. When writing the corresponding population balances, the nature of the attacking-attacked pair is relevant, making different the terms to be accounted for.

To better explain this point, let us discuss the kinetic terms resulting from a transesterification event involving an active and a dormant chain. (The case involving active chains is available in the referred literature.) In this case, (i) the dormant chain cannot be attacking and (ii) a portion of it is reactivated when attacked. Accordingly, the rate of formation of chains with n units is different for active and dormant chains: (i) an active chain R_n is formed when an active chain of any length is attacking a dormant chain with length larger than n; (ii) a dormant chain D_n is formed when a dormant chain of any length is attacked by an active chain with length smaller than n.

Finally, it should be noticed that such reactions are not affecting the number of both active and dormant chains in the system, but only the chain length of different chains produced by ROP reaction.

The reactions in Figure 13 can be formally expressed as

$$R_i + R_j \overset{k_x}{\leftrightarrows} R_{i+j-n} + R_n$$

$$R_i + D_j \overset{k_x}{\leftrightarrows} R_{i+j-n} + D_n$$

Such reactions have been introduced into the kinetic scheme of Figure 6, and the population balances have been modified accordingly. The resulting equations are the same as those in the previous version of the model (eqs 4−11) with the exception of the population balances of the active and dormant chains (eqs 8−10), which are rewritten as

$$\begin{aligned}\frac{dR_1}{dt} &= k_p M I - k_p M R_1 + k_d R_2 - k_d R_1 + k_{a1} D_1 C \\ &\quad - k_{a2} R_1 A - k_s R_1 ROH + k_s D_1 I - k_s R_1 \mu_0 + k_s D_1 \lambda_0 \\ &\quad - k_x (R_1(\lambda_1 - \lambda_0) - \lambda_0 \sum_{i=2}^{\infty} R_i + R_1(\mu_1 - \mu_0) - \lambda_0 \sum_{i=2}^{\infty} D_i) \end{aligned} \quad (25)$$

$$\begin{aligned}\frac{dR_n}{dt} &= k_p R_{n-1} M - k_p R_n M + k_d R_{n+1} - k_d R_n + k_{a1} D_n C \\ &\quad - k_{a2} R_n A - k_s R_n ROH + k_s D_n I - k_s R_n \mu_0 + k_s D_n \lambda_0 \\ &\quad - k_x (R_n(\lambda_1 - \lambda_0) - \lambda_0 \sum_{j=i+1}^{\infty} R_j + (n-1) R_n \lambda_0 - \\ &\quad \sum_{i=2}^{n-1} R_i \sum_{k=n+1-i}^{\infty} R_k + R_n(\mu_1 - \mu_0) - \sum_{i=2}^{n-1} R_i \sum_{k=n+1-i}^{\infty} D_k) \quad n \geq 2 \end{aligned} \quad (26)$$

$$\begin{aligned}\frac{dD_n}{dt} &= -k_{a1} D_n C + k_{a2} R_n A + k_s R_n ROH - k_s D_n I + k_s R_n \mu_0 \\ &\quad - k_s D_n \lambda_0 + k_x \lambda_0 \sum_{i=n+1}^{\infty} D_i - k_x (n-1) D_n \lambda_0 \end{aligned} \quad (27)$$

The resulting modified set of population balances has once more been solved by the method of moments, and the corresponding moment equations are reported in the Appendix.

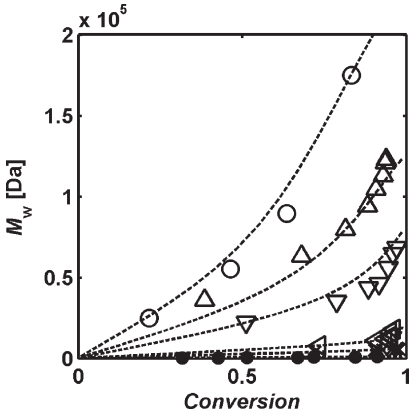

Figure 14. M_w versus conversion for LA polymerization with $Sn(Oct)_2$ and ROH. M/C = 3771, different ROH/C values. Experimental data: ○, 1; △, 5; ▽, 10; left tilted open triangles, 50; ×, 100; ●, = 565; model results, dashed lines.

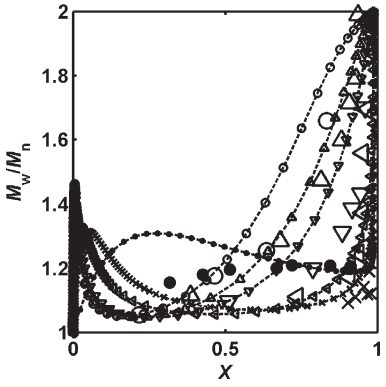

Figure 15. Dispersity versus conversion for LA polymerization with $Sn(Oct)_2$ and ROH. M/C = 3771, different ROH/C values. Experimental data: ○, 1; △, 5; ▽, 10; left tilted open triangles, 50; ×, 100; ●, 565; model results, dashed lines through symbols.

Note that a single new parameter is involved in the second version of the model, the rate coefficient k_x. The value of this quantity has been estimated by direct fitting of the model predictions to the experimental data, and the resulting best value is equal to 12 L mol^{-1} h^{-1}. The ratio between the propagation rate coefficient and this value, k_p/k_x = 246, has been compared with available literature data. For solution polymerization at 80 °C, Baran et al.[51] reported k_p/k_x = 200. Temperature increasing values have been indicated by Witzke[25] for bulk polymerization (300, 500, and 1300 at 160, 190, and 220 °C, respectively). The estimated ratio is very consistent in both cases keeping in mind the different temperatures, thus proving the reliability of the k_x value.

According to the eq 28

$$\frac{R_p}{R_x} = \frac{k_p M}{k_x R^*} \tag{28}$$

where R_x is the transesterification reaction rate, the ratio between the propagation rate and the transesterification rate shows that the transesterification reaction is slower than propagation. Because k_p, k_x, and R^* are constant, this ratio has the same profile as monomer concentration in the system. It will decrease as a linear function of monomer conversion. Accordingly, propagation is dominant at low conversion, whereas the transesterification reaction will broaden the molecular weight distribution at higher conversion only. The comparison between experimental results and model predictions is shown in Figures 14 and 15 for the experiments at different nominal ROH/C ratio. Because the exchange reaction is not affecting the polymerization rate and the number of chains, the results for the conversion rate and the number-average molecular weight are exactly the same as those of the first version of the model, already shown in Figures 9 and 10.

By inspection of the results, it is apparent that transesterification reactions increase the weight-average molecular weights in the right way, thus improving the model predictions in terms of dispersity. Namely, at small amounts of alcohol, dispersity quickly increases from the unity value typical of living conditions to an asymptotic value of 2. Such value was previously reported in

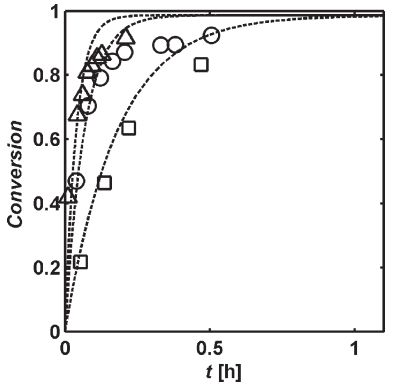

Figure 16. Conversion and Y versus time for LA polymerization with $Sn(Oct)_2$ and ROH. ROH/C = 1, different M/C values. Experimental data: □, 3771; ○, 1000; △, 500; model results, dashed lines.

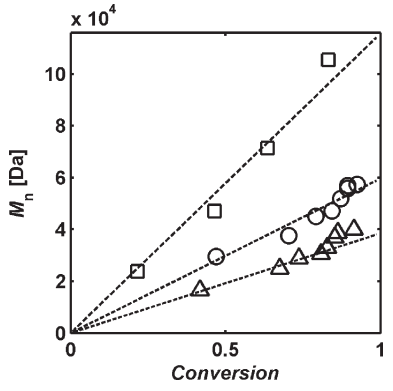

Figure 17. M_n versus conversion and time for LA polymerization with $Sn(Oct)_2$ and ROH. ROH/C = 1, different M/C values. Experimental data: □, 3771; ○, 1000; △, 500; model results, dashed lines.

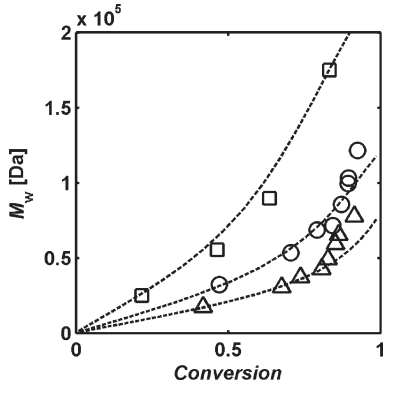

Figure 18. M_w versus conversion and time for LA polymerization with $Sn(Oct)_2$ and ROH. ROH/C = 1, different M/C values. Experimental data: □, 3771; ○, = 1000; △, 500; model results, dashed lines.

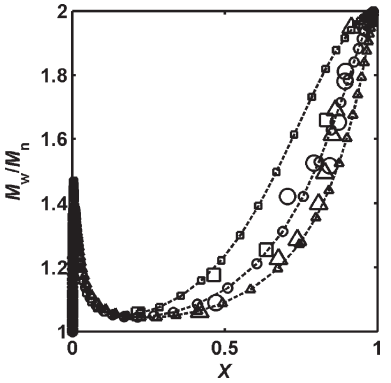

Figure 19. Dispersity versus conversion for LA polymerization with $Sn(Oct)_2$ and ROH. ROH/C = 1, different M/C values. Experimental data: □, 3771; ○, 1000; △, = 500; model results, dashed lines through symbols.

the literature[25,49] for systems dominated by exchange reactions, thus proving the reliability of the implemented scheme. At larger and larger OH amounts, the role of exchange reactions is reduced by the dominant transfer reactions, and the dispersity evolution typical of living systems is established.

Model Validation: Experiments at Different Catalyst Concentrations

To validate the model proposed in the last previous section, its prediction ability is checked here with respect to experiments at constant ratio ROH/C = 1 and different ratios M/C (Figures 4 and 5). The comparison between model predictions and experiments is summarized in Figures 16−19. Keeping in mind the genuinely predictive approach applied in this case, the agreement is quite satisfactory in terms of both conversion and molecular weight properties. Note that because of the small value of the ratio ROH/C, the role of the environmental impurities becomes especially important in this case. As usual, we accounted for such impurities in the model by increasing the initial concentration of alcohol according to the values in Table 3. The resulting agreement justifies such methodology.

Conclusions

A model of ROP of lactide carried out in bulk at 130 °C using $Sn(Oct)_2$ as catalyst and 1-dodecanol as cocatalyst is presented. A simplified version of a literature polymerization mechanism (alkoxide initiation[18,19]) has been used. Model validation and parameter evaluation were carried out by comparison with experimental data at different values of the molar ratios monomer−catalyst and catalyst−cocatalyst. The living nature of the reaction has been confirmed, along with the two-fold role of the alcoholic species, acting as cocatalyst and chain transfer agent at the same time. The value of the activation equilibrium constant has been estimated at 130 °C, indicating that a large excess of cocatalyst is needed to achieve complete catalyst activation. Moreover, inter-transesterification reactions have been included in the kinetic scheme to correctly predict the broadening of the molecular weight distribution. Such a reaction also involves the dormant chains, a reaction step fully neglected in all previous literature. The broadening due to these reactions is effectively contrasted by increasing the amount of cocatalyst, even if shorter chains are obviously obtained in this case.

Acknowledgment. The financial support provided by the Swiss Commission for Technology and Innovation (KTI/CTI; project no. 8611.2 PFIW-IW) is gratefully acknowledged

Appendix

Moment equations corresponding to the model accounting for activation, propagation, and reversible deactivation (eqs 8−10):

$$\frac{d\lambda_0}{dt} = k_{a1}\mu_0 C - k_{a2}\lambda_0 A + k_p MI - k_s\lambda_0 ROH + k_s\mu_0 I$$

$$\frac{d\lambda_1}{dt} = k_{a1}\mu_1 C - k_{a2}\lambda_1 A + k_p MI + k_p M\lambda_0 - k_d\lambda_0 - k_s\lambda_1 ROH + k_s\mu_1 I - k_s\lambda_1\mu_0 + k_s\mu_1\lambda_0$$

$$\frac{d\lambda_2}{dt} = k_{a1}\mu_2 C - k_{a2}\lambda_2 A + k_p MI + k_p M(2\lambda_1 + \lambda_0) + k_d(\lambda_0 - 2\lambda_1) - k_s\lambda_2 ROH + k_s\mu_2 I - k_s\lambda_2\mu_0 + k_s\mu_2\lambda_0$$

$$\frac{d\mu_0}{dt} = -k_{a1}\mu_0 C + k_{a2}\lambda_0 A + k_s\lambda_0 ROH - k_s\mu_0 I$$

$$\frac{d\mu_1}{dt} = -k_{a1}\mu_1 C + k_{a2}\lambda_1 A + k_s\lambda_1 ROH - k_s\mu_1 I + k_s\lambda_1\mu_0 - k_s\mu_1\lambda_0$$

$$\frac{d\mu_2}{dt} = -k_{a1}\mu_2 C + k_{a2}\lambda_2 A + k_s\lambda_2 ROH - k_s\mu_2 I + k_s\lambda_2\mu_0 - k_s\mu_2\lambda_0$$

Moment equations corresponding to the model including transesterification reactions (eqs 25−27):

$$\frac{d\lambda_0}{dt} = k_{a1}\mu_0 C - k_{a2}\lambda_0 A + k_p MI - k_s\lambda_0 ROH + k_s\mu_0 I$$

$$\frac{d\lambda_1}{dt} = k_{a1}\mu_1 C - k_{a2}\lambda_1 A + k_p MI + k_p M\lambda_0 - k_d\lambda_0 - k_s\lambda_1 ROH + k_s\mu_1 I - k_s\lambda_1\mu_0 + k_s\mu_1\lambda_0 - k_x\lambda_1(\mu_1 - \mu_0) + \frac{1}{2}k_x\lambda_0(\mu_2 - \mu_1)$$

$$\frac{d\lambda_2}{dt} = k_{a1}\mu_2 C - k_{a2}\lambda_2 A + k_p MI + k_p M(2\lambda_1 + \lambda_0) + k_d(\lambda_0 - 2\lambda_1) - k_s\lambda_2 ROH + k_s\mu_2 I - k_s\lambda_2\mu_0 + k_s\mu_2\lambda_0 + \frac{1}{3}k_x\lambda_0(\lambda_1 - \lambda_3) + k_x\lambda_1(\lambda_2 - \lambda_1) - k_x\lambda_2(\mu_1 - \mu_0) + \frac{1}{6}k_x\lambda_0(2\mu_3 - 3\mu_2 + \mu_1)$$

$$\frac{d\mu_0}{dt} = -k_{a1}\mu_0 C + k_{a2}\lambda_0 A + k_s\lambda_0 ROH - k_s\mu_0 I$$

$$\frac{d\mu_1}{dt} = -k_{a1}\mu_1 C + k_{a2}\lambda_1 A + k_s\lambda_1 ROH - k_s\mu_1 I + k_s\lambda_1\mu_0 - k_s\mu_1\lambda_0 + k_x\lambda_1(\mu_1 - \mu_0) - \frac{1}{2}k_x\lambda_0(\mu_2 - \mu_1)$$

$$\frac{d\mu_2}{dt} = -k_{a1}\mu_2 C + k_{a2}\lambda_2 A + k_s\lambda_2 ROH - k_s\mu_2 I + k_s\lambda_2\mu_0 - k_s\mu_2\lambda_0 + k_x\lambda_2(\mu_1 - \mu_0) + k_x\lambda_1(\mu_2 - \mu_1) + \frac{1}{6}k_x\lambda_0(-4\mu_3 + 3\mu_2 + \mu_1)$$

along with the corresponding closure formula[52]

$$\lambda_3 \cong \frac{\lambda_2(2\lambda_2\lambda_0 - {\lambda_1}^2)}{\lambda_1\lambda_0}$$

References and Notes

(1) Gilding, D. K.; Reed, A. M. *Polymer* **1979**, *20*, 1459–1464.
(2) Vert, M.; Li, S.; Spenlehauer, G.; Guerin, P. *J. Mater. Sci.: Mater. Med.* **1992**, *3*, 432–446.
(3) Duncan, R.; Kopecek, J. *Adv. Polym. Sci.* **1984**, *57*, 51–101.
(4) Mainil−varlet, P.; Rahm, R.; Gogolewski, S. *Biomaterials* **1997**, *18*, 257–266.
(5) Hartmann, M. H. In *Biopolymers from Renewable Resources*; Kaplan, D. L., Ed.; Springer-Verlag: Berlin, 1998; pp 367−411.
(6) Auras, R.; Harte, B.; Selke, S. *Macromol. Biosci.* **2004**, *4*, 835–864.
(7) Teeters, W. O. (Du Pont, Erf.) U.S. Patent 2,362,511, **1944**.
(8) Filachione, E. M.; Fisher, C. H. *Ind. Eng. Chem.* **1944**, *36*, 223–228.
(9) Moona, S.−I.; Leeb, C.−W.; Taniguchia, I.; Miyamotoa, M.; Kimura, Y. *Polymer* **2001**, *42*, 5059–5062.
(10) Carothers, W. H.; Dorough, G. L.; van Natta, F. J. *J. Am. Chem. Soc.* **1932**, *54*, 761–772.
(11) Schneider, K. A. (Du Pont, Erf.) U. S. Patent 2,703,316, **1955**.
(12) Kleine, J.; Kleine, H. H. *Die Makromol. Chem.* **1959**, *30*, 23–38.
(13) Lunt, J. *Polym. Degrad. Stab.* **1998**, *59*, 145–152.
(14) Jacobsen, S.; Degee, Ph.; Fritz, H. G.; Dubois, Ph.; Jerome, R. *Polym. Eng. Sci.* **1999**, *39*, 1311–1319.
(15) Drumright, R. E.; Gruber, P. R.; Henton, D. E. *Adv. Mater.* **2000**, *12*, 1841–1846.
(16) Datta, R.; Henry, M. *J. Chem. Technol. Biotechnol.* **2006**, *81*, 1119–1129.
(17) Mehta, R.; Kumar, V.; Bhunia, H.; Upadhyay, S. N. *J. Macromol. Sci., Part C: Poly. Rev.* **2005**, *45*, 325–349.
(18) Kowalski, A.; Duda, A.; Penczek, S. *Macromolecules* **2000**, *33*, 7359–7370.
(19) Duda, A.; Penczek, S. Chapter 12. In *Biopolymers: Polyesters II: Properties and Chemical Synthesis*; Doi, Y., Steinbüchel, A., Eds.; Wiley-VCH: Weinheim, Germany, 2002; Volume *3b*; pp 371−430.
(20) Kricheldorf, H. R.; Kreiser−Saunders, I.; Boettecher, C. *Polymer* **1995**, *36*, 1253–1250.
(21) Kricheldorf, H. R.; Kreiser−Saunders, I.; Stricker, A. *Macromolecules* **2000**, *33*, 702–709.
(22) Eenink, M. J. D. *Synthesis of Biodegradable Polymers and Development of Biodegradable Hollow Fibers for the Controlled Release of Drugs*. Ph.D. Thesis, Technische Hogeschool Twente Enschede, Enschede, The Netherlands, 1987.
(23) Zhang, X.; Macdonald, D. A.; Goosen, M. F. A.; Mcauley, K. B. *J. Polym. Sci., Part A: Polym. Chem.* **1994**, *32*, 2965–2970.
(24) Witzke, D. R.; Narayan, R.; Kolstad, J. J. *Macromolecules* **1997**, *30*, 7075–7085.
(25) Witzke, D. R. *Introduction to Properties, Engineering, and Prospects of Polylactide Polymers*. Ph.D. Dissertation, Michigan State University, East Lansing, MI, **1997**.
(26) Puaux, J. P.; Banu, I.; Nagy, I.; Bozga, G. *Macromol. Symp.* **2007**, *259*, 318–326.
(27) Mehta, R.; Kumar, V.; Upadhyay, S. N. *Polym.−Plast. Technol. Eng.* **2007**, *46*, 933–937.
(28) Mehta, R.; Kumar, V.; Upadhyay, S. N. *Polym.−Plast. Technol. Eng.* **2007**, *46*, 257–264.
(29) Schwach, G.; Coudane, J.; Engel, R.; Vert, M. *J. Polym. Sci., Part A: Poly. Chem.* **1997**, *35*, 3431–3440.
(30) Rudin, A. In *Elements of Polymer Science & Engineering: An Introductory Text and Reference for Engineers and Chemists*, 2nd ed.; Academic Press: San Diego, 1998; p 107.
(31) Garlotta, D. *J. Polym. Environ.* **2001**, *9*, 63–84.
(32) Schindler, A.; Harper, D. *J. Polym. Sci., Poly. Chem. Ed.* **1979**, *17*, 2593–2599.
(33) Dorgan, J. R.; Janzen, J.; Knauss, D. M.; Hait, S. B.; Limoges, B. R.; Hutchinson, M. H. *J. Polym. Sci., Part B: Polym. Phys.* **2005**, *43*, 3100–3111.
(34) Kurata, M.; Tsunashima, Y. In *Polymer Handbook*, 4th ed.; Brandrup, J., Immergut, E. H., Grulke, E. A., Abe, A., Bloch, D. R., Eds.; Wiley-Interscience: New York, 1999; Vol. *VII*, p 22.
(35) Engelberg, I.; Kohn, J. *Biomaterials* **1991**, *12*, 292–304.
(36) Mano, J. F.; Wang, Y.; Viana, J. C.; Denchev, Z.; Oliveira, M. J. *Macromol. Mater. Eng.* **2004**, *289*, 910–915.
(37) Miyata, T; Masuko, T. *Polymer* **1998**, *39*, 5515–5521.
(38) Liao, R.; Yang, B.; Yu, W.; Zhou, C. *J. Appl. Polym. Sci.* **2007**, *104*, 310–317.
(39) Cohn, D.; Younes, H.; Marom, G. *Polymer* **1987**, *28*, 2018–2022.
(40) Li, H.; Huneault, M. A. *Polymer* **2007**, *48*, 6855–6866.
(41) Iannace, S.; Nicolais, L *J. Appl. Polym. Sci.* **1997**, *64*, 911–919.
(42) Migliaresi, C.; De Lollis, A.; Fambri, L.; Cohn, D. *Clin. Mater.* **1991**, *8*, 111–118.
(43) Lundberg, R. D.; Cox, E. F. In *Ring-Opening Polymerization*; Frisch, K. C., Reegen, S. L., Eds.; Dekker: New York, 1969; pp 247−302.
(44) Odian, G. Chapter 7. In *Principles of Polymerization*, 4th ed.; John Wiley & Sons: Hoboken, NJ, ; pp 562−563.
(45) Nijenhuis, A. J.; Grijpma, D. W.; Pennings, A. J. *Macromolecules* **1992**, *25*, 6419–6424.
(46) Ramjit, H. G.; Sedgwick, R. D. *J. Macromol. Sci., Chem.* **1976**, *A10*, 815–824.
(47) Kotliar, A. M. *J. Polym. Sci., Part D: Macromol. Rev.* **1981**, *16*, 367–395.
(48) Lertola, J. G. *J. Polym. Sci., Part A: Polym. Chem.* **1990**, *28*, 2793–2807.
(49) Penczek, S.; Duda, A.; Szymanski, R. *Macromol. Symp.* **1998**, *132*, 441–449.
(50) Wachsen, O.; Reichert, K. H.; Krüger, R. P.; Much, H.; Schulz, G. *Polym. Degrad. Stab.* **1997**, *55*, 225–231.
(51) Baran, J.; Duda, A.; Kowalski, A.; Szymanski, R.; Penczek, S. *Macromol. Symp.* **1997**, *123*, 93–101.
(52) Hulburt, H. M.; Katz, S. *Chem. Eng. Sci.* **1964**, *19*, 555–574.